Acoustic Velocity Analogy Formulation for Sources in Quiescent Medium

JiaHua He
Northwestern Polytechnical University School of Aeronautics https://orcid.org/0000-0002-7615-1994
Sidan Xue
Northwestern Polytechnical University School of Aeronautics
QiuHong Liu (liuqh@nwpu.edu.cn)
Northwestern Polytechnical University School of Aeronautics
DangGuo Yang
China Aerodynamics Research and Development Center
LiangQuan Wang
China Aerodynamics Research and Development Center

Research

Keywords: Acoustic analogy, Acoustic velocity, Penetrable surface, Quiescent medium, Vector wave equation

Posted Date: April 6th, 2022

DOI: https://doi.org/10.21203/rs.3.rs-1512488/v1

Acoustic Velocity Analogy Formulation for Sources in Quiescent Medium

Jiahua He[1], Sidan Xue[1], and Qiuhong Liu [1*]
Northwestern Polytechnical University, *Xi'an*, *710072*, *China*

Dangguo Yang[2] and Liangquan Wang[3]
China Aerodynamics Research and Development Center, *Mianyang*, *621000*, *China*

The prediction of acoustic scattering requires the acoustic velocity evaluation on the scattering surface in order to satisfy the boundary conditions. According to the idea of acoustic analogy, this paper induces a vector wave equation of aeroacoustics by rearranging the conversation equations of mass and momentum with a penetrable surface. Then, an analytical formulation of the acoustic velocity, called formulation V2A, is derived for sources in a quiescent medium by solving the vector wave equation with the free-space Green's function. The validity of the formulation is confirmed by numerical results for a stationary monopole, a stationary dipole source, and a rotating monopole source in quiescent medium. The result indicates that the predication of formulation V2A is identical to the exact solutions no matter in far-field or near-field.

Keywords: Acoustic analogy, Acoustic velocity, Penetrable surface, Quiescent medium, Vector wave equation

Nomenclature

A	=	amplitude of the velocity potential
c_∞	=	ambient speed of sound
d	=	rotation radius of a point source
$\mathbf{F}$	=	$\mathbf{n} \times (\rho \mathbf{u})$, vector
f	=	data surface function
G_0	=	free-space Green's function
g	=	retarded time function
$H(f)$	=	Heaviside function
k	=	wave number
L_i	=	loading source term

* Associate Professor, National Key Laboratory of Science and Technology on Aerodynamic Design and Research, liuqh@nwpu.edu.cn. (Corresponding Author)

l = radius of a spherical penetrable surface

M_i = source Mach number components

n_i = surface unit normal components

p = flow pressure

p' = pressure fluctuation

p_∞ = undisturbed flow pressure

Q = thickness source term

r = distance between observer and source

r_x = distance between observer and rotation centre

$\tilde{r}_i$ = radiation direction unit

T_{ij} = Lighthill's stress tensor

t = observer time

u_i = velocity of the fluid

v_i = velocity of the data surface

x_i = observer position components

y_i = source position components

$\boldsymbol{x}$ = position vector of the observer

$\boldsymbol{y}$ = position vector of the source

α = observer angle

δ = Dirac delta function

ρ = flow density

ρ_∞ = undisturbed flow density

ρ' = density fluctuation

ω = angular frequency

σ_{ij} = viscous stress tensor

τ = source time

ϕ = acoustic velocity potential

I.Introduction

Computational Aeroacoustics (CAA) is aimed at studying noise generation and propagation in medium commonly air. The most commonly used method in CAA is to simulate noise generation by high-fidelity fluid simulation in a limited region. And the acoustic field can be computed by solving a standard wave equation with the assumption that waves is linear propagation from the near field to the far field. This indirect method, known as acoustic analogy, was raised by Lighthill [1,2] in the classical research of jet noise. The Ffowcs-Williams and Hawkings (FW-H) equation

[3], with the monopole, dipole and quadrupole sources on the right-hand side (RHS), is the most popular method for acoustic problems involving a permeable or non-permeable integration surface in the source region. A complete solution to the FW-H equation consists of surface and volume integration parts. If the permeable integration surface is large enough, the sound generation, reflection and refraction can be involved in this surface, the contribution of quadrupole source can be ignored, hence monopoles and dipoles are the dominant sources [4]. As a result, the acoustic field outside of the integration surface can only be derived from the flow variables on the permeable surface, such as Farassat's Formulations 1 and 1A [5,6].

In the path of sound propagation, obstacle will interact with the acoustic wave to causes scattering, namely, secondary sound spread in a variety of directions. If the characteristic size of the scatterer (solid bodies, interfaces between different media, etc.) is much smaller than the acoustic wavelength, then all points of the scatterer surface correspond to the same sound field phase and the scatterer is called acoustically compact. Otherwise, it's acoustically non-compact. The interaction between the acoustic wave and the non-compact body will give rise to acoustic scattering, which changes the magnitude, waveform and directivity of the acoustic field. For example, the open rotor noise scattered by a center body [7,8] or a fuselage [9,10] and the jet noise scattered by wings [11,12] should be considered in a comprehensive aero-acoustic simulation. Various numerical methods, such as the boundary element method (BEM) [13,14] and the equivalent source method (ESM) [15,16], have been developed to solve the sound scattering problem with non-compact bodies. These methods require the magnitude of the acoustic pressure gradient or acoustic velocity on the scattering surface to satisfy the boundary conditions [17,18].

The acoustic pressure gradient can be used as the boundary condition because it is related to the acoustic velocity through the acoustic velocity potential. However, direct numerical computation for the acoustic pressure gradient is expensive. If an analytical formulation of the pressure gradient can be obtained, the computational effort can be appreciable reduced. A semi analytical formulation was proposed by Farassat and Brentner [19] to calculate the acoustic pressure gradient. Lee et al. [20] presented time-domain analytical formulae G1 and G1A for the pressure gradient prediction. Furthermore, the acoustic scattering of rotorcraft noise can be evaluated with the combination of the formulation G1A and the equivalent source method [21].

Ghorbaniasl et al. [22] derived time-domain analytical formulations V1 and V1A of the acoustic velocity for sources in arbitrary motion from the FW-H equation. The frequency domain version of the acoustic velocity formulae

named as FV1A and FV2A was obtained by Mao et al. [23] to compute the acoustic velocity for rotating sources. In addition, Mao et al. [24] proposed a vector wave equation for acoustic velocity, which enabled an alternative approach to derive the acoustic velocity formulae V1 and V1A. Lee et al. [25] further demonstrated that the acoustic velocity formulation can be obtained directly from the sound pressure gradient formulation. In the acoustic velocity formulae V1 and V1A, the calculation of loading source contains a time integration from 0 to an arbitrary observer time, which means that the initial conditions for the acoustic velocity are different from the FW-H equation. Therefore, Ghorbaniasl's formulae for acoustic velocity are mathematically inexact.

The current work is devoted to develop an analytical formulation of the acoustic velocity for sources in quiescent medium. Starting from the continuity and momentum equations with a penetrable surface and following the derivation procedure of the FW-H equation, a vector wave equation and its subsequent formulations for the acoustic velocity are developed in the time domain. The acoustic velocity formulation named as formulation V2A which is more compact than formulation V1A and simpler to implement. Formulation V2A is specifically designed to make efficient use of the nearfield data on the penetrable surface enclosing the acoustic sources.

The rest of the paper is organized as follows. In Sec. II, an acoustic velocity wave equation with compact form is derived and discussed. In Sec. III, the derivation of formulation V2A is presented. The numerical implementation and verification cases are discussed in Sec. IV. Conclusion are provided in Sec. V.

II.Vector wave equation

Consider that the motion of an acoustic perturbation in a homogeneous and stationary medium with density ρ_∞, pressure p_∞, and sound speed c_∞. The classical acoustic analogy theory is based on the conservation equations of mass and momentum written as

$$\frac{\partial \rho}{\partial t} + \nabla \cdot (\rho \boldsymbol{u}) = 0, \tag{1}$$

$$\frac{\partial (\rho \boldsymbol{u})}{\partial t} + \nabla \cdot (\rho \boldsymbol{u}\boldsymbol{u}) + \nabla p = \nabla \cdot \boldsymbol{\sigma}, \tag{2}$$

where ρ, $\mathbf{u}$, p and $\boldsymbol{\sigma}$ are the flow density, velocity, pressure and viscous stress tensor respectively.

The acoustic analogy involves enclosing the aerodynamic sources with a permeable surface that is described by a function $f = 0$. Assume that the function f is defined as follows: $f > 0$ represents the region outside the surface, $f < 0$ denotes the region enclosed by the data surface and $|\nabla f| = 1$ indicates the region on the surface. Thus, the

outward unit normal vector of the surface ($f = 0$) is $\mathbf{n} = \nabla f$. Then the continuity equation in the region outside the surface is

$$H(f)\left[\frac{\partial \rho^{'}}{\partial t} + \nabla \cdot (\rho \boldsymbol{u})\right] = 0, \tag{3}$$

where $\rho^{'} = \rho - \rho_{\infty}$ stands for the density fluctuation and $H(f)$ is the Heaviside function. Moving $H(f)$ inside the differential operators and using

$$\frac{\partial H(f)}{\partial t} = -\boldsymbol{v} \cdot \boldsymbol{n}\delta(f), \quad \nabla H(f) = \boldsymbol{n}\delta(f), \tag{4}$$

then

$$\frac{\partial}{\partial t}[H(f)\rho^{'}] + \nabla \cdot [H(f)\rho \boldsymbol{u}] = Q\delta(f), \tag{5}$$

with

$$Q = \rho(\boldsymbol{u} - \boldsymbol{v}) \cdot \boldsymbol{n} + \rho_{\infty}\boldsymbol{v} \cdot \boldsymbol{n}, \tag{6}$$

where vector $\mathbf{v}$ is the moving velocity of the non-deformable surface $f = 0$ and $\delta(f)$ denotes the Dirac function. Similarly, the conservation of momentum can be written as

$$\frac{\partial}{\partial t}[H(f)\rho \boldsymbol{u}] + c_{\infty}^{2}\nabla[H(f)\rho^{'}] = -\nabla \cdot [\boldsymbol{T}H(f)] + \boldsymbol{L}\delta(f) \tag{7}$$

with

$$\boldsymbol{T} = \rho \boldsymbol{u}\boldsymbol{u} + (p^{'} - c_{\infty}^{2}\rho^{'})\boldsymbol{I} - \boldsymbol{\sigma} \tag{8}$$

and

$$\boldsymbol{L} = \rho \boldsymbol{u}\{(\boldsymbol{u} - \boldsymbol{v}) \cdot \boldsymbol{n}\} + p^{'}\boldsymbol{n} - \boldsymbol{\sigma} \cdot \boldsymbol{n}, \tag{9}$$

where $p^{'} = p - p_{\infty}$ denotes the pressure fluctuation.

The vector $\rho\mathbf{u}$ is employed as the variable in the wave operator to derive the vector wave equation. Performing the gradient of equation (5) yields

$$\frac{\partial}{\partial t}\{\nabla[H(f)\rho^{'}]\} + \nabla\{\nabla \cdot [H(f)\rho \boldsymbol{u}]\} = \nabla[Q\delta(f)]. \tag{10}$$

Taking the temporal derivative of equation (7) and multiplying by the constant $1/c_{\infty}^{2}$, we obtain

$$\frac{1}{c_{\infty}^{2}}\frac{\partial^{2}}{\partial t^{2}}[H(f)\rho \boldsymbol{u}] + \frac{\partial}{\partial t}\{\nabla[H(f)\rho^{'}]\} = -\frac{1}{c_{\infty}^{2}}\frac{\partial}{\partial t}\{\nabla \cdot [\boldsymbol{T}H(f)]\} + \frac{1}{c_{\infty}^{2}}\frac{\partial}{\partial t}[\boldsymbol{L}\delta(f)]. \tag{11}$$

Equation (11) subtracted from equation (10) gives

$$\frac{1}{c_{\infty}^{2}}\frac{\partial^{2}}{\partial t^{2}}[H(f)\rho \boldsymbol{u}] - \nabla\{\nabla \cdot [H(f)\rho \boldsymbol{u}]\} = -\frac{1}{c_{\infty}^{2}}\frac{\partial}{\partial t}\{\nabla \cdot [\boldsymbol{T}H(f)]\} + \frac{1}{c_{\infty}^{2}}\frac{\partial}{\partial t}[\boldsymbol{L}\delta(f)] - \nabla[Q\delta(f)] \tag{12}$$

The left-hand side (LHS) of equation (12) is not a standard wave operator because the second term is not a Laplace

operator. We can rearrange equation (12) by making use of the vector identity

$$\begin{aligned}\nabla\{\nabla\cdot[H(f)\rho\mathbf{u}]\} &= \nabla\times\nabla\times[H(f)\rho\mathbf{u}] + \nabla^2[H(f)\rho\mathbf{u}] \\ &= \nabla\times[H(f)\nabla\times(\rho\mathbf{u})] + \nabla\times[\mathbf{F}\delta(f)] + \nabla^2[H(f)\rho\mathbf{u}]\end{aligned} \tag{13}$$

with $\mathbf{F} = \mathbf{n}\times(\rho\mathbf{u})$ to obtain a vector wave equation for acoustic velocity

$$\left(\frac{1}{c_\infty^2}\frac{\partial^2}{\partial t^2} - \nabla^2\right)[H(f)\rho\boldsymbol{u}] = \underbrace{\nabla\times[H(f)\nabla\times(\rho\boldsymbol{u})] - \frac{1}{c_\infty^2}\frac{\partial}{\partial t}\{\nabla\cdot[\boldsymbol{T}H(f)]\}}_{\text{Volume source}} + \underbrace{\tfrac{1}{c_\infty^2}\tfrac{\partial}{\partial t}[\boldsymbol{L}\delta(f)]}_{\text{Loading source}} + \underbrace{\nabla\times[\boldsymbol{F}\delta(f)] - \nabla[Q\delta(f)]}_{\text{Thickness source}}. \tag{14}$$

Equation (14) is an exact rearrangement of the basic equations of aerodynamics. It should be noted that this equation is more compact than the vector wave equation proposed by Mao [24]. More importantly, the formulation V2A does not rely on initial condition. The first two terms on the RHS of equation (18) represent the volume source. The third term denotes the loading source, and the last two terms correspond to the thickness source. The fourth term is treated as part of the thickness source since it directly comes from the continuity equation. The potential error in the proposed method depends on the value of the volume source, if the contribution of volume source is ignored in acoustic velocity evaluations. Fortunately, the value of the volume source is likely to be small outside the integration surface since the acoustic velocity is irrotational,

$$\nabla\times[H(f)\nabla\times(\rho\boldsymbol{u})] = \nabla\times[H(f)\nabla\rho'\times\boldsymbol{u}] = O(\varepsilon^2), \tag{15}$$

and the sound propagation is isentropic and inviscid,

$$\tfrac{1}{c_\infty^2}\tfrac{\partial}{\partial t}\{\nabla\cdot[\boldsymbol{T}H(f)]\} = \tfrac{1}{c_\infty^2}\tfrac{\partial}{\partial t}\{\nabla\cdot[\rho\boldsymbol{u}\boldsymbol{u}]\} = O(\varepsilon^2). \tag{16}$$

In general, the density fluctuation ρ' is usually much smaller than ρ_∞ outside the source region, which leads to an approximation of $\rho\mathbf{u} = \left(\rho_\infty + \rho'\right)\mathbf{u} \approx \rho_\infty\mathbf{u}$. Applying the free space Green's function $G_0(\boldsymbol{x},\boldsymbol{y},t-\tau)$, the integral solution of equation (14) can be written as

$$\rho_\infty\boldsymbol{u}(\boldsymbol{x},t) = \int_{-\infty}^{t}\int_{\mathbb{R}}\{\nabla\times[\boldsymbol{F}\delta(f)] - \nabla[Q\delta(f)]\}G_0\,d^3\boldsymbol{y}d\tau + \tfrac{1}{c_\infty^2}\tfrac{\partial}{\partial t}\int_{-\infty}^{t}\int_{\mathbb{R}}\boldsymbol{L}\delta(f)G_0\,d^3\boldsymbol{y}d\tau. \tag{17}$$

III.Acoustic velocity formulations

The free space Green's function is the fundamental solution to the wave equation and its analytical expression is

$$G_0(\mathbf{x},\mathbf{y},t-\tau) = \frac{\delta(g)}{4\pi r},\ g = \tau - t + \frac{r}{c_\infty} \tag{18}$$

where **x** and **y** denote the coordinates of the observer and source points. t and τ are times at observer and source locations, respectively. The variable r is defined as

$$\mathbf{r} = \mathbf{x} - \mathbf{y}, r = |\mathbf{r}| \tag{19}$$

A. Formulation V2

The loading noise u_{Li} and the thickness noise u_{Ti} contributions are obtained from

$$4\pi\rho_\infty u_{Li}(\boldsymbol{x}, t) = \frac{1}{c_\infty^2}\frac{\partial}{\partial t}\int_{-\infty}^{t}\int_{\mathbb{R}} L_i\delta(f)\frac{\delta(g)}{r}d^3\boldsymbol{y}d\tau \tag{20}$$

and

$$4\pi\rho_\infty u_{Ti}(\boldsymbol{x}, t) = \frac{\partial}{\partial x_j}\int_{-\infty}^{t}\int_{\mathbb{R}} E_{ij}\delta(f)\frac{\delta(g)}{r}d^3\boldsymbol{y}d\tau - \frac{\partial}{\partial x_i}\int_{-\infty}^{t}\int_{\mathbb{R}} Q\delta(f)\frac{\delta(g)}{r}d^3\boldsymbol{y}d\tau, \tag{21}$$

respectively, where $E_{ij} = \varepsilon_{ijk}F_k$.

In order to integrate over $d\tau$, the method of generalized function theory is used

$$\int_{-\infty}^{t} h(\tau)\delta(g)d\tau = \left[\frac{h(\tau)}{\partial g/\partial\tau}\right]_{g=0} \tag{22}$$

where $h(\tau)$ is an arbitrary smooth function and the notation $[\cdot]_{g=0}$ denotes evaluation of the term in brackets at the root of $g = 0$. If g has more than one root, the term is computed at each root and the final solution is the sum of the evaluated terms. When the source is in subsonic motion, the root of g is called as retarded time,

$$\tau = t - \frac{r}{c_\infty}. \tag{23}$$

The partial differentiation of g with respect to τ can be evaluated as

$$\frac{\partial g}{\partial\tau} = 1 + \frac{1}{c_\infty}\frac{\partial r}{\partial\tau} = 1 - \frac{1}{c_\infty}\frac{\partial r}{\partial x_j}\frac{\partial y_j}{\partial\tau} = 1 - M_r, \tag{24}$$

where M_r is defined as

$$M_r = \frac{1}{c_\infty}\frac{\partial y_j}{\partial\tau}\tilde{r}_i = \frac{v_i}{c_\infty}\tilde{r}_i = M_i\tilde{r}_i. \tag{25}$$

On the other hand, the combination of

$$\frac{\partial}{\partial x_i}\left\{\frac{\delta(g)}{r}\right\} = \frac{\partial g}{\partial x_i}\frac{\delta'(g)}{r} - \frac{\delta(g)}{r^2}\frac{\partial r}{\partial x_i} = \frac{\tilde{r}_i}{rc_\infty}\delta'(g) - \frac{\tilde{r}_i}{r^2}\delta(g) \tag{26}$$

and

$$\frac{\tilde{r}_i}{r}\delta'(g) = -\frac{\partial}{\partial t}\left(\frac{\tilde{r}_i}{r}\delta(g)\right) \tag{27}$$

yields

$$\frac{\partial}{\partial x_i}\left\{\frac{\delta(g)}{r}\right\} = -\frac{1}{c_\infty}\frac{\partial}{\partial t}\left(\frac{\tilde{r}_i}{r}\delta(g)\right) - \frac{\tilde{r}_i}{r^2}\delta(g). \tag{28}$$

Hence, equations (20) and (21) can be simplified to

$$4\pi\rho_\infty u_{Li}(\boldsymbol{x},t) = \frac{1}{c_\infty^2}\frac{\partial}{\partial t}\int_{f=0}\left[\frac{L_i}{r(1-M_r)}\right]_{\text{ret}} d^2\boldsymbol{y}, \tag{29}$$

$$4\pi\rho_\infty u_{Ti}(\boldsymbol{x},t) = \frac{1}{c_\infty}\frac{\partial}{\partial t}\int_{f=0}\left[\frac{Q\tilde{r}_i - E_{ij}\tilde{r}_j}{r(1-M_r)}\right]_{\text{ret}} d^2\boldsymbol{y} + \int_{f=0}\left[\frac{Q\tilde{r}_i - E_{ij}\tilde{r}_j}{r^2(1-M_r)}\right]_{\text{ret}} d^2\boldsymbol{y}. \tag{30}$$

As much, equations (29) and (30) are called formulation V2, being the analogous to formulation V1 of Ghorbaniasl for the acoustic velocity. In formulation V2, the observer temporal derivatives are outside the integral.

B. Formulation V2A

The next modification consists of moving the temporal derivative inside the integrals. This can be made based on the retarded time definition given in equation (23) and the following rule

$$\frac{\partial\tau}{\partial t} = 1 - \frac{1}{c_\infty}\frac{\partial r}{\partial\tau}\frac{\partial\tau}{\partial t} = 1 + M_r\frac{\partial\tau}{\partial t}. \tag{31}$$

From (31), we have

$$\frac{\partial}{\partial t} = \left[\frac{1}{1-M_r}\frac{\partial}{\partial\tau}\right]_{\text{ret}}. \tag{32}$$

Taking the temporal derivate inside the integral of the loading source and using (32) yields

$$4\pi\rho_\infty u_{Li}(\boldsymbol{x},t) = \frac{1}{c_\infty^2}\int_{f=0}\frac{1}{1-M_r}\frac{\partial}{\partial\tau}\left[\frac{L_i}{r(1-M_r)}\right]_{\text{ret}} d^2\boldsymbol{y}. \tag{33}$$

It can be rewritten as

$$4\pi\rho_\infty u_{Li}(\boldsymbol{x},t) = \frac{1}{c_\infty^2}\int_{f=0}\left[\frac{\dot{L}_i}{r(1-M_r)^2}\right]_{ret} d^2\boldsymbol{y} - \frac{1}{c_\infty^2}\int_{f=0}\left[\frac{L_i\dot{r}}{r^2(1-M_r)^2}\right]_{ret} d^2\boldsymbol{y} + \frac{1}{c_\infty^2}\int_{f=0}\left[\frac{L_i}{r(1-M_r)^3}\frac{\partial M_r}{\partial\tau}\right]_{\text{ret}} d^2\boldsymbol{y}. \tag{34}$$

which time partial derivative term is written with a dot on its top.

Substituting

$$\dot{r} = -M_r c_\infty, \quad \frac{\partial M_r}{\partial\tau} = \dot{M}_r + \frac{c_\infty}{r}(M_r^2 - M^2) \tag{35}$$

into equation (34) yields

$$4\pi\rho_\infty u_{Li}(\boldsymbol{x},t) = \frac{1}{c_\infty^2}\int_{f=0}\left[\frac{1}{r(1-M_r)^2}\left(\dot{L}_i + \frac{L_i\dot{M}_r}{1-M_r}\right)\right]_{\text{ret}} d^2\boldsymbol{y} + \frac{1}{c_\infty}\int_{f=0}\left[\frac{L_i(M_r - M^2)}{r^2(1-M_r)^3}\right]_{\text{ret}} d^2\boldsymbol{y}. \tag{36}$$

Applying relation (32) to equation (30) in the following expression

$$4\pi\rho_\infty u_{Ti}(\boldsymbol{x},t) = \frac{1}{c_\infty}\int_{f=0}\frac{1}{1-M_r}\frac{\partial}{\partial\tau}\left[\frac{Q\tilde{r}_i - E_{ij}\tilde{r}_j}{r(1-M_r)}\right]_{\text{ret}} d^2\boldsymbol{y} + \int_{f=0}\left[\frac{Q\tilde{r}_i - E_{ij}\tilde{r}_j}{r^2(1-M_r)}\right]_{\text{ret}} d^2\boldsymbol{y}. \tag{37}$$

On the RHS of equation (37), taking the temporal derivative gives

$$\frac{\partial}{\partial\tau}\left[\frac{Q\tilde{r}_i-E_{ij}\tilde{r}_j}{r(1-M_r)}\right]=\frac{\dot{Q}\tilde{r}_i+Q\dot{\tilde{r}}_i-\dot{E}_{ij}\tilde{r}_j-E_{ij}\dot{\tilde{r}}_j}{r(1-M_r)}-\frac{(Q\tilde{r}_i-E_{ij}\tilde{r}_j)\dot{r}}{r^2(1-M_r)}+\frac{Q\tilde{r}_i-E_{ij}\tilde{r}_j}{r(1-M_r)^2}\frac{\partial M_r}{\partial\tau}, \tag{38}$$

with

$$\dot{\tilde{r}}_i=c_\infty\frac{\tilde{r}_iM_r-M_i}{r}. \tag{39}$$

Therefore, equation (37) becomes

$$4\pi\rho_\infty u_{Ti}(\boldsymbol{x},t)=\frac{1}{c_\infty}\int_{f=0}\left[\frac{\dot{Q}\tilde{r}_i+Q\dot{\tilde{r}}_i-\left(\dot{E}_{ij}\tilde{r}_j+E_{ij}\dot{\tilde{r}}_j\right)}{r(1-M_r)^2}\right]_{\text{ret}}d^2\boldsymbol{y}+\int_{f=0}\left[\frac{Q\tilde{r}_i-E_{ij}\tilde{r}_j}{r^2(1-M_r)}\right]_{\text{ret}}d^2\boldsymbol{y}$$
$$+\frac{1}{c_\infty}\int_{f=0}\left[\frac{Q\tilde{r}_i-E_{ij}\tilde{r}_j}{r(1-M_r)^3}\frac{\partial M_r}{\partial\tau}\right]_{\text{ret}}d^2\boldsymbol{y}-\frac{1}{c_\infty}\int_{f=0}\left[\frac{(Q\tilde{r}_i-E_{ij}\tilde{r}_j)\dot{r}}{r^2(1-M_r)^2}\right]_{\text{ret}}d^2\boldsymbol{y}. \tag{40}$$

Using relation (35) and rearranging the terms, we have

$$4\pi\rho_\infty u_{Ti}(\boldsymbol{x},t)=\frac{1}{c_\infty}\int_{f=0}\left[\frac{1}{r(1-M_r)^2}\left\{\tilde{r}_i\left(\dot{Q}+\frac{Q\dot{M}_r}{1-M_r}\right)-\tilde{r}_j\left(\dot{E}_{ij}+\frac{E_{ij}\dot{M}_r}{1-M_r}\right)\right\}\right]_{\text{ret}}d^2\boldsymbol{y}$$
$$+\int_{f=0}\left[\frac{(Q\tilde{r}_i-E_{ij}\tilde{r}_j)(1-M^2)}{r^2(1-M_r)^3}-\frac{QM_i-E_{ij}M_j}{r^2(1-M_r)^2}\right]_{\text{ret}}d^2\boldsymbol{y} \tag{41}$$

Equations (36) and (41) are named as formulation V2A, being analogous to the formulation V1A of Ghorbaniasl. In the fixed permeable surface case, the emission distance r, the local normal vector components n_i and the source velocity $v_i=0$ are constant and do not vary with time. Therefore, the emission time can be obtained with an explicit solution. The formulations of (36) and (41) can be reduced to

$$4\pi\rho_\infty u_{Li}(\boldsymbol{x},t)=\frac{1}{c_\infty^2}\int_{f=0}\left[\frac{\dot{L}_i}{r}\right]_{\text{ret}}d^2\boldsymbol{y} \tag{42}$$

$$4\pi\rho_\infty u_{Ti}(\boldsymbol{x},t)=\frac{1}{c_\infty}\int_{f=0}\left[\frac{\tilde{r}_i\dot{Q}-\tilde{r}_j\dot{E}_{ij}}{r}\right]_{\text{ret}}d^2\boldsymbol{y}+\int_{f=0}\left[\frac{Q\tilde{r}_i-E_{ij}\tilde{r}_j}{r^2}\right]_{\text{ret}}d^2\boldsymbol{y} \tag{43}$$

IV.Validation Examples

In this section, the canonical problems of sound radiation by a monopole, a dipole and a moving monopole in a quiescent medium were solved for the numerical verification of the proposed acoustic velocity formulation V2A. The numerical results were compared with corresponding analytical solutions. The source terms were computed over a fictitious, closed surface surrounding the source. The acoustic code was written on the basis of the advanced time algorithm [26]. In order to focus on the acoustic velocity formulation V2A and its implementation, and to avoid any bias related to the accuracy of the flow-field simulation, all the required flow properties on the permeable surface,

such as the pressure, density, velocity and the corresponding temporal derivatives, were obtained from the exact solution of the flow field generated by the source. These properties were then used as the input to the acoustic code. It should be noted that the nonlinear terms in the thickness and loading sources were omitted since these problems are purely linear. In all test cases, the mesh resolution of the permeable surface and the time step are chosen such that the wavelength and period of the radiated wave are resolved with at least 32 points to ensure the accuracy of the numerical solutions.

A. Stationary monopole in a quiescent medium

The acoustic field of a fixed monopole in a quiescent medium can be characterized by a simple harmonic velocity potential function

$$\phi(\boldsymbol{x}, t) = \frac{A}{4\pi r} exp\left[i\omega\left(t - \frac{r}{c_\infty}\right)\right]. \tag{55}$$

The monopole source was located at the origin of the coordinate system. The amplitude of the velocity potential was $A = 1m^2/s$. The speed of sound was $c_\infty = 340m/s$. The wave number was $k = \omega/c_\infty = 1.0$. For a time period 256 timesteps were used to describe the source. A closed spherical surface with radius $l = 0.5m$ and 7840 panels was adopted as the data collection surface. The observers were placed on a circle on the x_1-x_2 plane with a geometrical distance of $2l$ and $20l$ from the source. Predictions by the acoustic velocity formulation V1A of Ghorbaniasl were also implemented, and the results were also included for comparison.

The far-field with $r = 20l$ time period results among formulation V1A, V2A and exact solution are revealed in Figure 1 and Figure 2 with observer direction $\alpha = 60°$ and $\alpha = 230°$ respectively (the angle between the source and the observer measured from the x_1-axis). Both of the numerical methods show identical with the exact solution in the far-field.

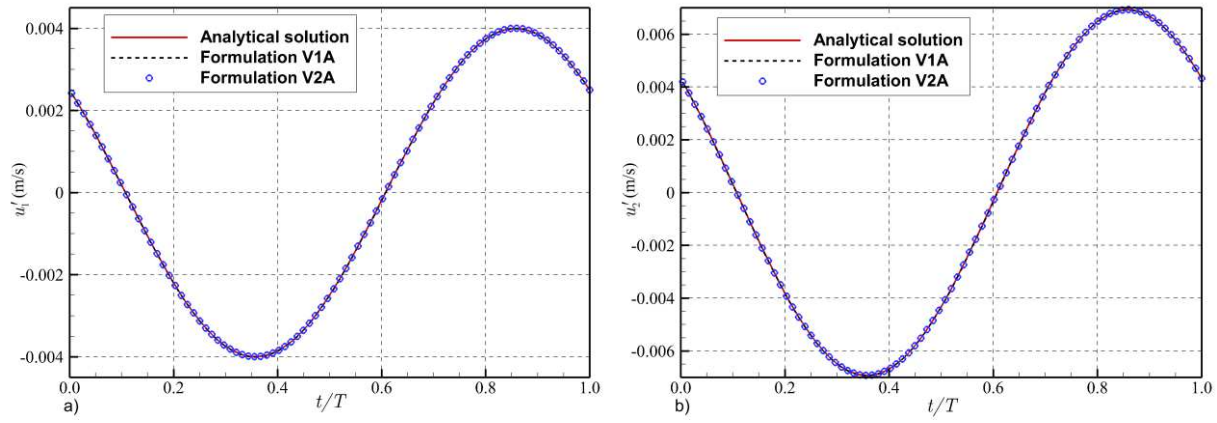

Figure 1 Comparison of monopole acoustic velocity predicted by V1A and V2A with that of the analytical solutions in x_1 (a) and x_2 (b) directions at $r = 20l$ with $\alpha = 60°$.

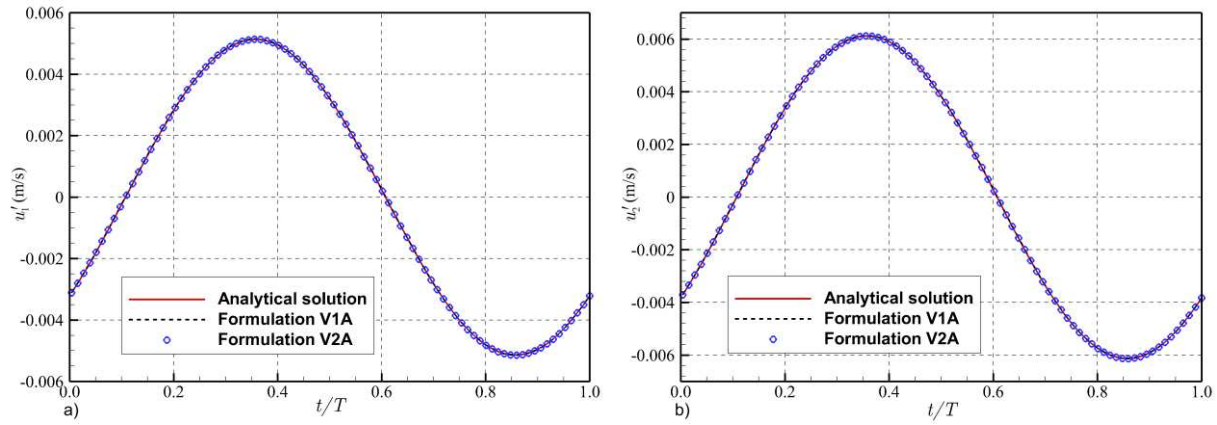

Figure 2 Comparison of monopole acoustic velocity predicted by V1A and V2A with that of the analytical solutions in x_1 (a) and x_2 (b) directions at $r = 20l$ with $\alpha = 230°$.

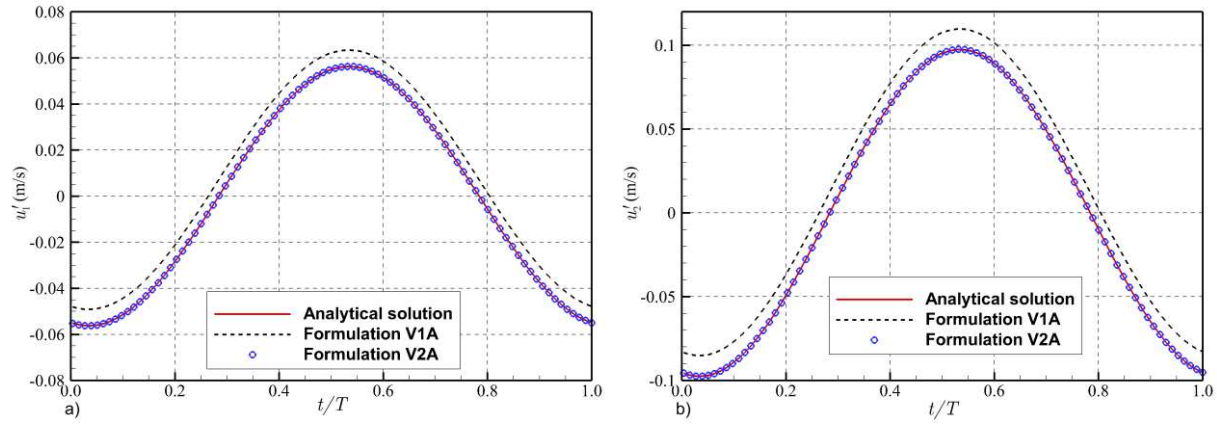

Figure 3 Comparison of monopole acoustic velocity predicted by V1A and V2A with that of the analytical solutions in x_1 (a) and x_2 (b) directions at $r = 2l$ with $\alpha = 60^{\circ}$.

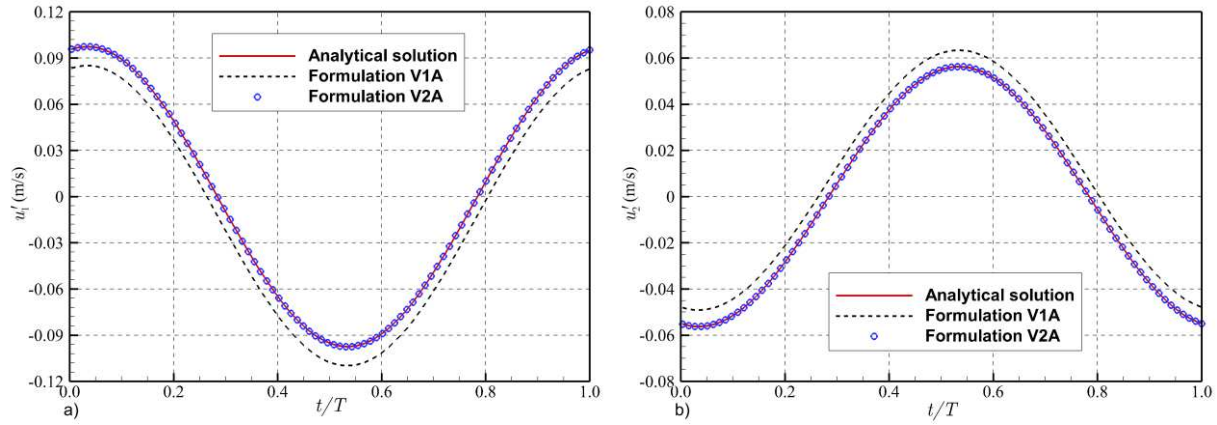

Figure 4 Comparison of monopole acoustic velocity predicted by V1A and V2A with that of the analytical solutions in x_1 (a) and x_2 (b) directions at $r = 2l$ with $\alpha = 150^{\circ}$.

However, the acoustic analogy applies in principle for observer locations in both the far-field and the near-field, and involves no far-field or near-field approximation. In practical applications, there are many situations that the distance between the source and the scatterer is not large enough to treat the observer field as far-field. In these conditions the far-field analysis is not valid, consequently a near-field analysis is necessary.

The near field results with $r = 2l$ are revealed in Figure 3 and Figure 4 with different observer. Figure 3 compares the time histories of the acoustic velocity in x_1 and x_2 components obtained with formulations V1A, V2A and exact solution at the observer angle $\alpha = 60^{\circ}$. It shows that formulation V1A has obviously difference with the exact solution in the near field. The predictions of formulation V2A are in a good agreement with the analytical solutions. Figure 4 provides the outcome of another observer in direction $\alpha = 150°$ with $r = 2l$. The result also shows that the formulation V2A has a better predication than formulation V1A because in formulation V1A the initial condition of time integration is incorrect. In the far-field, the influence of initial condition in formulation V1A becomes unimportant as presented before.

B. Stationary dipole in a quiescent medium

The second validation test case is a stationary dipole point source located in a quiescent medium. The dipole axis is aligned with the x_2-axis. From the extended form of the velocity potential of the aforementioned monopole case, we can obtain the velocity potential for such dipole case as follows,

$$\phi(\boldsymbol{x}, t) = \frac{\partial}{\partial x_2}\left\{\frac{A}{4\pi r} exp\left[i\omega\left(t - \frac{r}{c_\infty}\right)\right]\right\}. \tag{56}$$

The same potential amplitude, sound speed and wavenumber as test case 1 were prescribed. The induced acoustic

velocity was recorded at distance of $r = 2l$ and $r = 20l$ in different direction from the source. l is the radius of permeable surface as mentioned in test case 1.

A spherical permeable surface with 7840 panels was created to enclose the point source. In order to reduce the computational effort, 128 observer time points were used per period which is enough to describe the source. The calculation was performed for this test case, and the acoustic velocity components were computed with formulation V2A and formulation V1A. The predictions were compared with those of the analytical solution.

The acoustic velocity obtained by far-field observer located at $r = 20l$ and direction $\alpha = 30°$ and $\alpha = 230°$ are shown in Figure 5 and Figure 6 respectively. The numerical and analytical methods match each other quite well.

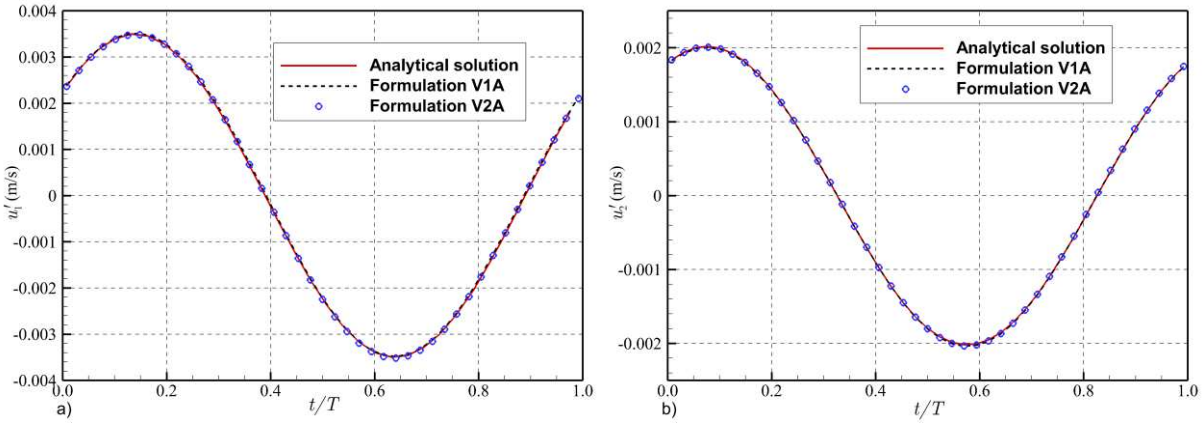

Figure 5 Comparison of dipole acoustic velocity predicted by V1A and V2A with that of the analytical solutions in x_1 (a) and x_2 (b) directions at $r = 20l$ with α =30° .

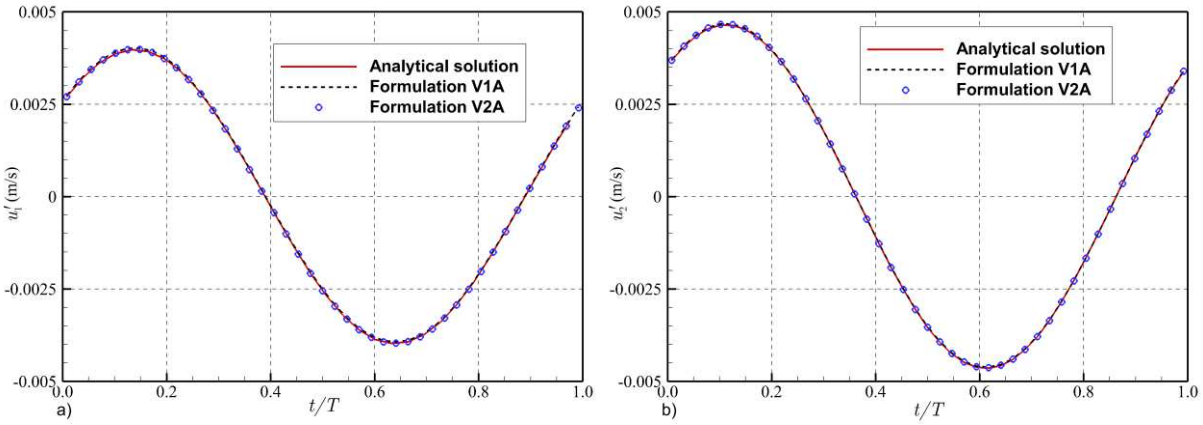

Figure 6 Comparison of dipole acoustic velocity predicted by V1A and V2A with that of the analytical solutions in x_1 (a) and x_2 (b) directions at $r = 20l$ with $\alpha = 230°$

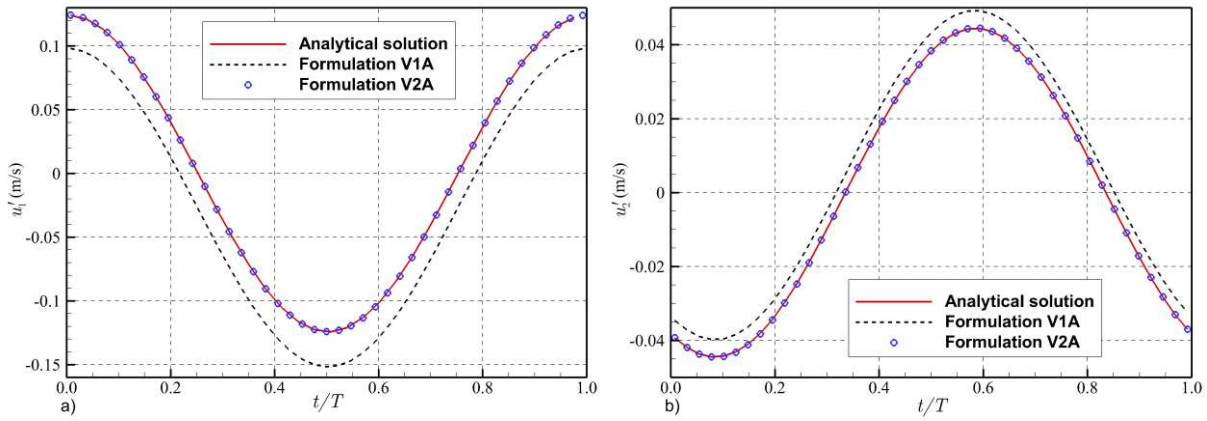

Figure 7 Comparison of dipole acoustic velocity predicted by V1A and V2A with that of the analytical solutions in x_1 (a) and x_2 (b) directions $r = 2l$ with $\alpha = 30^{\circ}$.

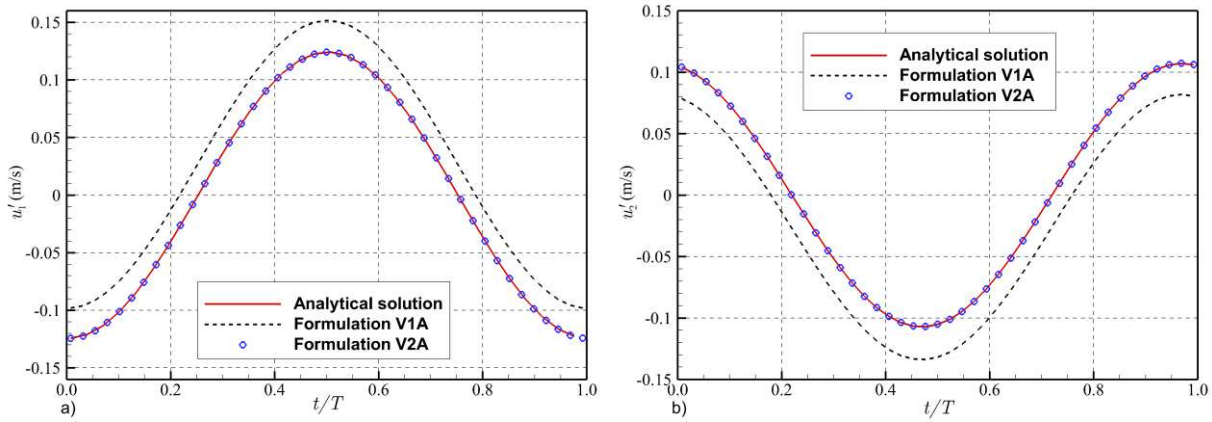

Figure 8 Comparison of dipole acoustic velocity predicted by V1A and V2A with that of the analytical solutions in x_1 (a) and x_2 (b) directions at $r = 2l$ and $\alpha = 120^{\circ}$.

Figure 7 shows the time histories of the acoustic velocity in x_1 and x_2 components at the observer angle $\alpha = 30^{\circ}$ and radius $r = 2l$. The numerical prediction of formulation V2A and the exact solution yield nearly identical results, but the prediction of formulation V1A has some difference in the near-field. In the observer direction of $\alpha = 120°$ shown in Figure 8 also indicates the same phenomenon.

C. Rotating monopole in a quiescent medium

The last test case is a monopole point source rotating in a quiescent medium as shown schematically in Figure 9. This case was designed to validate the accuracy of formulation V2A to predict the general case of sound radiated by moving sources similar to the thickness source term of a fan or a helicopter rotor blade. The monopole source rotates counter-clockwise around the x_3-axis shown in Figure 9 with a constant angular frequency $\Omega = 0.25\omega$, a constant radius $d = 0.25m$, and an initial azimuth angle of zero. The velocity potential for such monopole is

$$\phi(\boldsymbol{x}, t) = \left[\frac{A}{4\pi r(1-M_r)} exp\left\{i\omega\left(t - \frac{r}{c_\infty}\right)\right\}\right]_{\text{ret}} \tag{57}$$

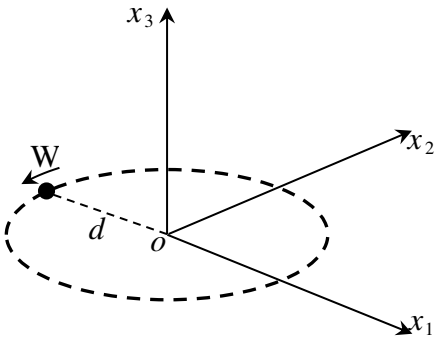

Figure 9 The schematic of a rotating monopole in a quiescent medium.

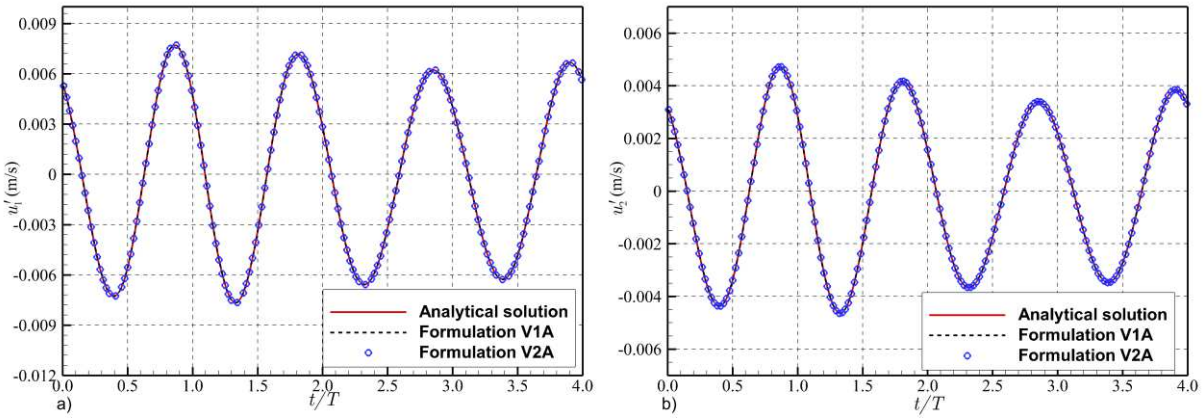

Figure 10 Comparison of the time histories of the numerical acoustic velocity generated by a rotating monopole with the analytical solutions at $r = 20l$ and $\alpha = 30^{\circ}$. (a) x_1-component of acoustic velocity; (b) x_2-component of acoustic velocity

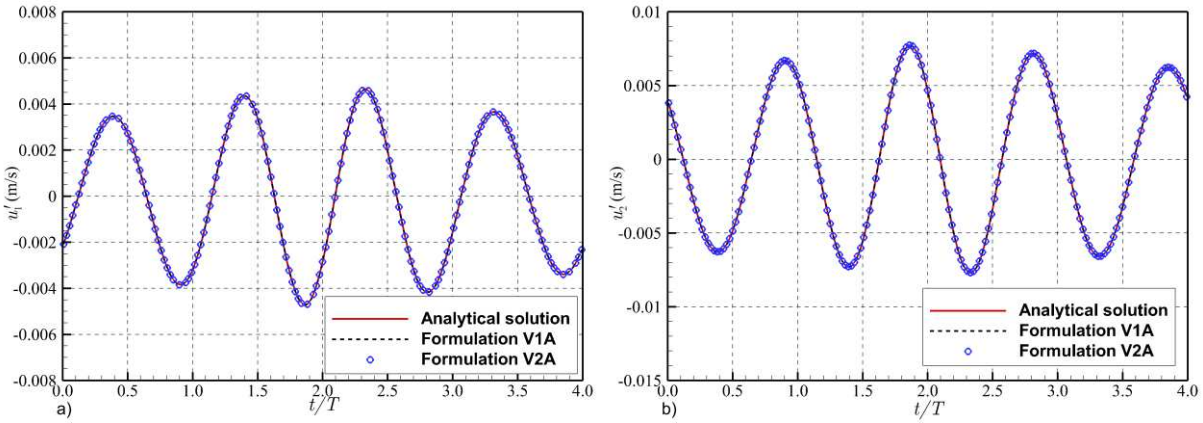

Figure 11 Comparison of the time histories of the numerical acoustic velocity generated by a rotating monopole with the analytical solutions at $r = 20l$ and $\alpha = 120^{\circ}$. (a) x_1-component of acoustic velocity; (b) x_2-component of acoustic velocity

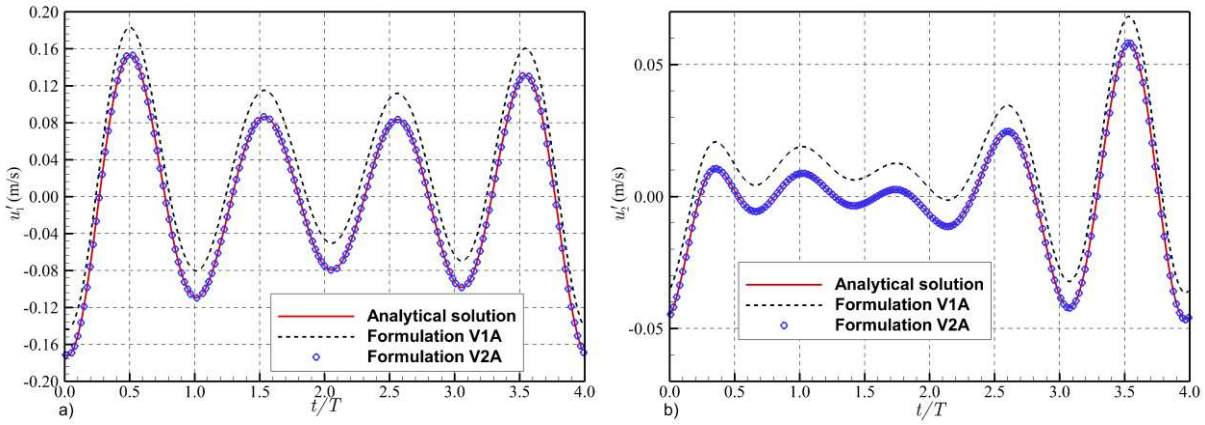

Figure 12 Comparison of the time histories of the numerical acoustic velocity generated by a rotating monopole with the analytical solutions at $r = 2l$ and $\alpha = 10^{\circ}$. (a) x_1-component of acoustic velocity; (b) x_2-component of acoustic velocity.

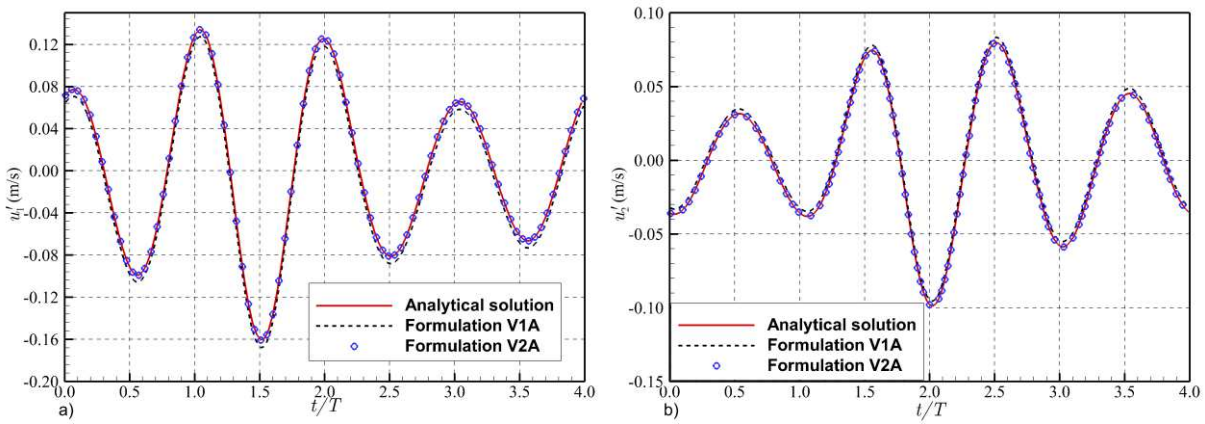

Figure 13 Comparison of the time histories of the numerical acoustic velocity generated by a rotating monopole with the analytical solutions at $r = 2l$ and $\alpha = 150^{\circ}$. (a) x_1-component of acoustic velocity; (b) x_2-component of acoustic velocity

A closed cylindrical surface was created as the data collection surface which has radius $l = 0.5m$ as mentioned in case 1 and case 2. The amplitude of the velocity potential and the pulsation frequency were the same as the previous test cases. The near-field observers are placed on a circle on the x_1-x_2 plane with a distance of $r = 2l$ from the rotation center and the far-field observer are placed on the same plane with $r = 20l$ from the rotation center.

Figure 10 and Figure 11 give the comparison in V1A, V2A and analytical solution in far-field with $r = 20l$. As other cases shown above, in the far-field, both numerical methods (formulation V1A and formulation V2A) can obtain good result.

Figure 12 shows the time history of the acoustic velocity perceived by an observer in the near-field with angle $\alpha = 10^{\circ}$. Excellent agreement between the predictions and the exact solution confirms the validity of formulation V2A and

its implementation, while formulation V1A shows some difference in the near-field in this direction. The result got through another observer in direction $\alpha = 150°$ in Figure 13 shows that the numerical result calculate by V2A is in good agreement with analytical solution and the result of V1A has just a little difference with analytical result.

V.Conclusions

The conservation equations of mass and momentum with a penetrable surface were rearranged to induce a vector wave equation of aeroacoustics. With this vector wave equation and the free-space Green's function, a time domain formulation named as formulation V2A was proposed for the calculation of the acoustic velocity field generated by sources in a quiescent medium.

Formulation V2A is suitable for the advanced time algorithm to reduce storage and computation requirements. The validity of formulation V2A is confirmed by the canonical test cases of a monopole and a dipole in a quiescent medium. Furthermore, the test case for a rotating monopole in a quiescent medium was also investigated. A permeable data surface was used in all cases, and the required flow properties on the permeable surface were obtained from the exact solution of the flow field generated by the source. The numerical predictions of formulation V2A were in very good agreement with the exact solutions no matter in far-field or near-field. It should be noted that the formulation V2A is only valid for quiescent medium now. Future work will be done to develop new acoustic velocity formulations suitable for moving medium.

Acknowledgments

N/A

Authors' contributions

The research output comes from a joint effort. All authors read and approved the final manuscript.

Funding

The research was supported by the National Natural Science Foundation of China under Grant No.11672244, Rotor Aerodynamics Key Laboratory under Grant No. 2112RAL202103-4 and the Foundation of National Key Laboratory under Grant No. JZX7Y202001SY002101-614220120030101.

Availability of data and materials

The datasets used and/or analyzed during the current study are available from the corresponding author upon reasonable requests.

Declarations

Competing interests

The authors declare that they have no competing interests.

Author details

1. National Key Laboratory of Science and Technology on Aerodynamic Design and Research, Northwestern Polytechnical University, Xi'an Shaanxi 710072, China.

2. State Key Laboratory of Aerodynamics, China Aerodynamics Research and Development Center, Mianyang Sichuan 621000, China.

3. Rotor Aerodynamics Key Laboratory, China Aerodynamics Research and Development Center, Mianyang Sichuan 621000, China.

References

[1] Lighthill, M. J., "On Sound Generated Aerodynamically. I. General Theory," *Proceedings of the Royal Society of London Series A*, Vol. 211, No. 1107, 1952, pp. 564-587.
doi: 10.1098/rspa.1952.0060

[2] Lighthill, M. J., "On Sound Generated Aerodynamically. II. Turbulence as a Source of Sound," *Proceedings of the Royal Society of London Series A*, Vol. 222, No. 1148, 1954, pp. 1-32.
doi: 10.1098/rspa.1954.0049

[3] Ffowcs Willianms J. E., and Hawkings, D. L., "Sound Generation by Turbulence and Surfaces in Arbitrary Motion," *Philosophical Transactions of the Royal Society A*, Vol. 264, No. 1151, 1969, pp. 321-342.
doi: 10.1098/rsta.1969.0031

[4] Brentner, K. S., and Farassat, F., "Analytical Comparison of the Acoustic Analogy and Kirchhoff Formulation for Moving Surfaces," *AIAA Journal*, Vol. 36, No. 8, 1998, pp. 1379-1386.
doi: 10.2514/2.558

[5] Farassat, F., "Derivation of Formulations 1 and 1A of Farassat," NASA TM-2007-214853, 2007.

[6] Farassat, F., "Linear Acoustic Formulas for Calculation of Rotating Blade Noise," *AIAA Journal*, Vol. 19, No. 9, 1981, pp. 1122–1130.

doi:10.2514/3.60051

[7] Kingan, M. J., and Self, R. H., "Open Rotor Tone Scattering," *Journal of Sound and Vibration*, Vol. 331, No.8, 2012, pp. 1806-1828.
doi: 10.1016 /j.jsv.2011.12 .001

[8] Kingan, M. J., and Sureshkumar, P., "Open Rotor Centrebody Scattering," *Journal of Sound and Vibration*, Vol. 333, No.2, 2014, pp. 418-433.
doi: 10.1016 /j.jsv.2013.08 .010

[9] Gennaretti, M., Bernardini, G., Poggi, C., and Testa, C., "Velocity-Potential Boundary-Field Integral Formulation for Sound Scattered by Moving Bodies," *AIAA Journal*, Vol. 56, No.9, 2018, pp. 3547-3557.
doi: 10.2514 /1.J056491

[10] Gaffney, J., McAlpine, A., Kingan, M. J., "A theoretical model of fuselage pressure levels due to fan tones radiated from the intake of an installed turbofan aero-engine," *Journal of the Acoustical Society of America*, Vol. 143, No.6, 2018, pp. 3394-3405.
doi: 10.1121/1.5038263

[11] Lyu, B., Dowling, A. P., and Naqavi, I., "Prediction of Installed Jet Noise," *Journal of Fluid Mechanics*, Vol. 811, 2017, pp. 234-268.
doi: 10.1017/jfm.2016.747

[12] Dawson, M. F., Lawrence, J. L. T., Self R. H., and Kingan, M. J., "Validation of a Jet-Surface Interaction Noise Model in Flight," *AIAA Journal*, Vol. 58, No.3, 2020, pp. 1130-1139.
doi: 10.2514/1.J058639

[13] Croaker, P., Kessissoglou, N., and Marburg, S., "Aeroacoustic Scattering Using a Particle Accelerated Computational Fluid Dynamics/Boundary Element Technique," *AIAA Journal*, Vol. 54, No.7, 2016, pp. 2116-2133.
doi: 10.2514/1.J054260

[14] Bernardini, G., Poggi, C., Gennaretti, M., and Testa, C., "Study of Velocity-Potential Integral Formulations for Sound Scattered by Moving Bodies," *AIAA Journal*, Vol. 59, No.3, 2021, pp. 1008-1019.
doi: 10.2514/1.J059482

[15] Lee, S., Brentner, K. S., and Morris, P. J., "Acoustic Scattering in the Time Domain Using an Equivalent Source Method," *AIAA Journal*, Vol. 48, No.12, 2010, pp. 2772-2780.
doi: 10.2514/1.45132

[16] Xu, C., Mao, Y. J., and Hu Z. W., "Improved Equivalent Source Method to Predict Sound Scattered by Solid Surfaces," *AIAA Journal*, Vol. 57, No.2, 2019, pp. 513-520.
doi: 10.2514/1.J057490

[17] Dunn, M. H., and Tinetti, A. F., "Aeroacoustic Scattering via the Equivalent Source Method," *AIAA 10th AIAA/CEAS Aeroacoustics Conference*, AIAA Paper 2004-2937, May 2004.

[18] Gennaretti, M., and Testa, C., "A Boundary Integral Formulation for Sound Scattered by Moving Bodies," *Journal of Sound and Vibration*, Vol. 314, Nos. 3–5, 2008, pp. 712–737.

doi:10.1016/j.jsv.2008.01.028

[19] Farassat, F., and Brentner, K. S., "The Derivation of the Gradient of the Acoustic Pressure on a Moving Surface for Application to the Fast Scattering Code (FSC)," NASA Technical Report TM-2005-213777, 2005.

[20] Lee, S. K., Brentner, K. S., Farassat, F., and Morris, P. J., "Analytic Formulation and Numerical Implementation of an Acoustic Pressure Gradient Prediction," *Journal of Sound and Vibration*,Vol. 319, Nos. 3-5, 2009, pp. 1200-1221.
doi:10.1016/j.jsv.2008.06.028

[21] Lee, S., Brentner, K. S., and Morris, P. J., "Time-Domain Approach for Acoustic Scattering of Rotorcraft Noise," *Journal of the American Helicopter Society*, Vol. 57, No. 4, 2012, pp. 1-12.
doi:10.4050/JAHS.57.042001

[22] Ghorbaniasl, G., Carley, M., and Lacor, C., "Acoustic Velocity Formulation for Sources in Arbitrary Motion," *AIAA Journal*, Vol. 51, No. 3, 2013, pp. 632-642.
doi:10.2514/1.J051958

[23] Mao, Y. J., Zhang, Q. L., Xu, C., and Qi, D. T., "Two Types of Frequency-Domain Acoustic Velocity Formulations for Rotating Thickness and Loading Sources," *AIAA Journal*, Vol. 53, No. 3, 2015, pp. 713-722.
doi:10.2514/1.j053230

[24] Mao, Y. J., Tang, H. T., and Xu, C., "Vector Wave Equation of Aeroacoustics and Acoustic Velocity Formulations for Quadrupole Source," *AIAA Journal*, Vol. 54, No. 6, 2016, pp. 1922-1931.
doi: 10.2514/1.J054687

[25] Lee, S., and Brentner, K. S., "Comment on 'Acoustic Velocity Formulation for Sources in Arbitrary Motion'," *AIAA Journal*, Vol. 54, No. 5, 2016, pp. 1809-1810.
doi: 10.2514/1.J054845

[26] Casalino, D., "An advanced time approach for acoustic analogy predictions," *Journal of Sound and Vibration*, Vol. 264, No.4, 2003, pp. 583-612.
doi: 10.1016/S0022-460X(02)00986-0